Large magnetic anisotropy and tunneling anisotropic magnetoresistance in layered bimetallic nanostructures: Case study of Mn/W(001)

A. B. Shick,[1] F. Máca,[1] M. Ondráček,[1] O. N. Mryasov,[2] and T. Jungwirth[3]
[1]*Institute of Physics, ASCR, Na Slovance 2, Prague 8, Czech Republic*
[2]*Seagate Research, Pittsburgh, Pennsylvania 15222, USA*
[3]*Institute of Physics, ASCR, Cukrovarnicka 10, Prague 6, Czech Republic*
and School of Physics and Astronomy, University of Nottingham, Nottingham NG7 2RD, United Kingdom
(Received 19 May 2008; revised manuscript received 3 July 2008; published 11 August 2008)

We predict large magnetic anisotropy energy (MAE) and tunneling anisotropic magnetoresistance in bimetallic 3*d*-4(5)*d* transition-metal structures which properly balance conditions to maximize moment on the magnetic 3*d* atom, exchange coupling between the 3*d* and 4(5)*d* elements, and magnetic susceptibility and spin-orbit coupling of the 4(5)*d* metal. Our *ab initio* MAE value of 5.57 meV/Mn atom and relative density-of-states anisotropies of ~100% in the ferromagnetic state of Mn overlayer on W(001) surface demonstrate that the optimal structures may contain unconventional combinations of transition metals. Results are interpreted by employing element and layer specific torque calculations of the MAE. It is shown that large MAE mainly comes from itinerant 5*d*(W)-atom magnetic moments at the interface and subinterface which are induced by exchange coupling with localized 3*d*(Mn)-atom moments. To relate these highly anisotropic transition-metal structures to potential applications we also provide estimates of the Curie temperature and the magnetic recording density that can be achieved for system parameters corresponding to our model ferromagnetic Mn/W(001) structure.

DOI: 10.1103/PhysRevB.78.054413 PACS number(s): 85.75.Mm, 75.45.+j, 75.50.Cc

I. INTRODUCTION

Key limiting factors for the magnetic recording density, i.e., for the minimum feasible bit size, are the superparamagnetic transition in the media and the detection threshold of magnetoresistive sensors. The superparamagnetic behavior sets on when the ratio of the magnetic anisotropy energy (MAE) to the thermal energy k_BT becomes small, resulting in fluctuations of the magnetization orientation which erase recorded data in short times. The MAE of Co-based transition-metal materials, used currently in hard disk media, is of a few tenths of meV per magnetic atom. Larger uniaxial magnetocrystalline anisotropies of up to 0.8 meV/atom have been predicted[1] for tetragonally strained FeCo alloys, followed by promising attempts to realize these structures experimentally.[2] Prospect for order-of-magnitude enhancements of the MAE in transition metals has, however, remained limited so far to exotic structures such as the monatomic Co chain and Co adatom on Pt(111) surface with impractical Curie temperatures of ~5–15 K.[3]

The detection threshold of read heads is derived from the magnetic sensitivity and noise characteristic, and over the past 15 years the anisotropic magnetoresistance (AMR) and the tunneling magnetoresistance (TMR) (or giant magnetoresistance) sensors completely outperformed classical magnetoinductive devices. Recent observations of the tunneling anisotropic magnetoresistance (TAMR) effect in ferromagnetic semiconductors[4–6] and, subsequently, in transition-metal structures[7–10] have opened new opportunity to combine the assets of the two leading magnetoresistive sensor technologies. These experimental and theoretical works have established that the microscopic origin of the TAMR is derived from the magnetic anisotropy in the density of states (DOS) of the ferromagnetic electrode. Maximum TAMR ratios of approximately 15% have so far been achieved in Pt-terminated Co/Pt thin-film multilayers.[10] It has been also pointed out[7] that transition-metal systems with large magnetocrystalline anisotropies have typically large TAMRs as one might expect from the common spin-orbit coupling based origin of these two effects.

In the work reported here we analyze the key physical quantities determining the anisotropic magnetic characteristics of 3*d*-4(5)*d* metal systems making use of *ab initio* numerical calculations of the MAE and magnetic anisotropy of the DOS. We consider an unconventional transition-metal structure formed by a Mn monolayer on W(001) surface. These model calculations demonstrate that transition-metal ferromagnets still offer a large potential for increasing MAE and TAMR. The paper is organized as follows. In Sec. II A we calculate and compare total energies of the ferromagnetic and antiferromagnetic state of the Mn/W(001) structure. Sections II B and II C present numerical analysis and discussion of the leading contributions to the MAE; the DOS anisotropy calculations are reported in Sec. II D. Estimates of the Curie temperature and recording density in the considered ferromagnetic Mn/W(001) model system are given in Sec. II E. Section III contains concluding remarks on the nature of the ground state of Mn overlayer on W(001) surface and summary of the main results of the paper.

II. RESULTS AND DISCUSSION

A. Ferromagnetic vs antiferromagnetic state of Mn/W(001)

It was recently reported by Ferriani *et al.*[11] that the ferromagnetic (FM) state of Mn/W(001) has lower total energy than the anti-FM-$c(2\times2)$ state. Following Ref. 11, we performed supercell calculations for Mn overlayer on W(001)

 ©2008 The American Physical Society

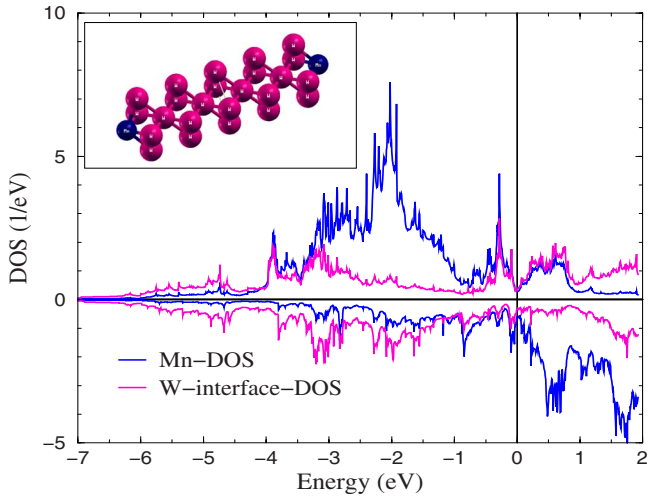

FIG. 1. (Color online) Main panel: spin-resolved PDOS for Mn and interface W layers. Inset: a schematic crystal structure used to represent the Mn chain at the W(001) surface.

surface, employing the standard VASP-PAW method[12] without spin-orbit coupling (SOC) and making use of generalized gradient approximation. A supercell model similar to Ref. 11 is used which consists of a nine-layer W(001) substrate with the $c(2\times2)$ two-dimensional (2D) unit cell and Mn monolayers on each side of the substrate (see the inset in Fig. 1). In order to find the lowest-energy magnetic configuration, the FM and anti-FM $[c(2\times2), p(2\times1)]$ Mn overlayer structures were considered. The in-plane interatomic distance of pure W (5.98 a.u.) was adopted. The interplane distances between Mn atom and W surface as well as within the substrate were allowed to relax in the calculations.

The total-energy difference $E_{\mathrm{AFM}}-E_{\mathrm{FM}}=0.183$ eV/Mn atom is obtained for the $c(2\times2)$ structure, in good agreement with the value of ~0.2 eV/Mn atom reported in Ref. 11. However, important differences compared to Ref. 11 are found for the relaxed atomic positions. For the FM case, we obtain a relatively large (~10.8%) relaxation of the interlayer distance d(Mn-W)=2.67 a.u. This value differs from d(Mn-W)=2.85 a.u. obtained in Ref. 11. Very small (practically negligible) changes in W-substrate atom positions are obtained. For the anti-FM case, smaller relaxation of d(Mn-W)=2.82 a.u. is found which is again different from the reported value of 2.97 a.u. in Ref. 11. In addition, the distance between interface and subinterface W layers is reduced by ~0.1 a.u. and practically no changes in remaining W-substrate layer positions are found in our calculations.

For the $p(2\times1)$ structure, we obtain the total-energy difference $E_{\mathrm{AFM}}-E_{\mathrm{FM}}=0.046$ eV/Mn atom. For the anti-FM $p(2\times1)$ case, we find d(Mn-W)=2.58 a.u., i.e., a 13.8% relaxation which is even larger than in the FM case. Again, we find practically no changes in the W-substrate atom positions.

The present results for structure relaxation together with energy difference between different FM and AFM states are in almost perfect agreement with previous calculations of Dennler and Hafne.[13] The origin of the quantitative difference between VASP-PAW results and FLEUR calculations can be explained noticing that no full relaxation is performed in Ref. 11. They varied and minimized the distance between Mn overlayer and W substrate while fixing the substrate atoms positions. The highly accurate full-potential linearized augmented plane-wave (FP-LAPW) (Ref. 14) method calculations using WIEN2K implementation[15] and the atomic positions obtained from VASP for the FM case yield nonzero forces of 8.2 mRy/a.u. for Mn, 5.9 mRy/a.u. for W-interface, −1.9 mRy/a.u. for W-subinterface, and 0.4 mRy/a.u. for W-subsubinterface layers which were relaxed. These forces are somewhat bigger than 1–2 mRy/a.u., which is commonly accepted value for "zero" force at equilibrium atomic position, meaning that VASP and FLAPW would yield slightly different structure relaxations. Still, the differences in the atomic positions will be on the scale not exceeding 0.1 a.u. Below we will show numerically that it will have no significant impact on the calculated values of the MAE.

TABLE I. Spin (M_S) and orbital (M_L) magnetic moments in Bohr magnetons for the magnetization along the z and x axes for the Mn atom at the surface, W atoms at the interface (I), and next-to-interface (I-1) layers; MAE=E_x-E_z in meV/Mn atom as a function of the number of k points in the full BZ.

z axis	Mn	W(I)	W(I-1)
M_S	3.176	−0.343	0.072
M_L	0.087	−0.055	−0.013
x axis	Mn	W(I)	W(I-1)
M_S	3.174	−0.342	0.073
M_L	0.073	−0.011	−0.009
No. of k points	1600	3600	4624
MAE	5.75	5.56	5.56

B. Magnetocrystalline anisotropy energy

In this section we investigate the relativistic electronic and magnetic properties of Mn/W(001). We use the relativistic version of the FP-LAPW, in which spin-orbit (SO) coupling is included in a self-consistent second-variational procedure.[16] The conventional (von Barth-Hedin) local-spin-density approximation is adopted in the calculations, which is expected to be valid for itinerant metallic systems.

We first employ the magnetic force theorem[17] to evaluate the MAE. Starting from self-consistent charge and spin densities calculated for the magnetic moment aligned along one of the principal axes, the moment is rotated and a single energy-band calculation is performed for the new orientation of the moment. Importantly, the same set of k points has to be used for the integration over the Brillouin zone (BZ) for accurate evaluation of the MAE.

The spin M_S and orbital M_L magnetic moments for two directions of the magnetization along the z and x axes are given in Table I for the Mn atom, W atoms at the interface (I), and next-to-interface (I-1) layers. There is a strong M_S(W) right at the interface which is antiparallel to M_S(Mn).

This is a typical behavior of $3d/5d$ systems with less than half-filled $5d$ shell, which differs from the behavior of (Fe,Co)/Pt bimetallic systems. The spin-resolved projected density of states (PDOS) for the Mn layer and the interfacial W layer is shown in Fig. 1, again illustrating the opposite spin splittings of Mn-PDOS and W-PDOS. The magnetic moment on W and the W-PDOS spin splitting oscillates and quickly decay when moving further from the interface. Still, small spin and orbital moments, $M_S(\mathrm{W}) \sim -0.06\ \mu_B$ and $M_L(\mathrm{W}) \sim 0.01\ \mu_B$, remain for the central W layer of the slab (see the insert in Fig. 1) due to a finite-size supercell used in the calculations.

Rotating the magnetization from the z to x axis produces practically no anisotropy in M_S for both Mn and W. M_L, on the other hand, shows a pronounced anisotropy with the larger value along the z axis. We also note the formal violation of the third Hund's rule for the W atoms at the interface as their M_S and M_L moments are not antialigned. This observation is in qualitative agreement with available experimental data for FM-Fe/W(110) (Ref. 18) and indicates that the magnetic moment on W is induced by the exchange interaction with the neighboring Mn layer.

The obtained positive MAE (see Table I) corresponds to the easy axis oriented along the z direction. The convergence for the MAE value with respect to the BZ integration was reached near 3600 k points in the 2D-BZ. The magnitude of the MAE of 5.57 meV/Mn atom is found remarkably large. To examine the sensitivity of the MAE to the Mn-W geometry, we performed additional calculations making use of the relaxed lattice parameters from Ref. 11 and found a comparably large MAE of 4.97 meV/Mn atom for 3600 k points in the 2D-BZ. The shape anisotropy due to the dipole-dipole interaction gives an additional contribution to the MAE,[19] $E_{\mathrm{dd}} = -0.12$ meV/Mn atom.

C. Element-specific contributions to MAE

We now discuss alternative MAE calculations based on the torque method,[20] which provide useful insight into the origin of the large MAE we observe in the Mn/W(001) system. The technique has been employed in Korringa-Kohn-Rostoker (KKR) and linear muffin-tin orbitals (LMTO)-based calculations in the atomic sphere approximation as a complementary approach to the commonly used magnetic force theorem. The torque method has been first implemented in FP-LAPW basis in Ref. 21. Importantly, using this approach allows us to split the total MAE into contributions from different species in the unit cell. The calculated torque $T(\theta,\phi) = dE(\theta,\phi)/d\theta$ is shown in Fig. 2(a) as a function of the polar angle θ corresponding to the x-z-plane ($\phi = 0$) rotation and in Fig. 2(b) as a function of the angle ϕ for fixed $\theta = \frac{\pi}{4}$. A set of k points equivalent to 3600 k points in the full 2D-BZ is used in the calculations. The total MAE $= \int_0^{\pi/2} d\theta T(\theta, \phi = 0) = 5.41$ meV/Mn atom obtained from these torque calculations is in a very good agreement with the magnetic force theorem MAE=5.57 meV/Mn atom (see Table I).

For the tetragonal symmetry case, the phenomenological total-energy dependence on the magnetization direction reads (up to the fourth-order terms)

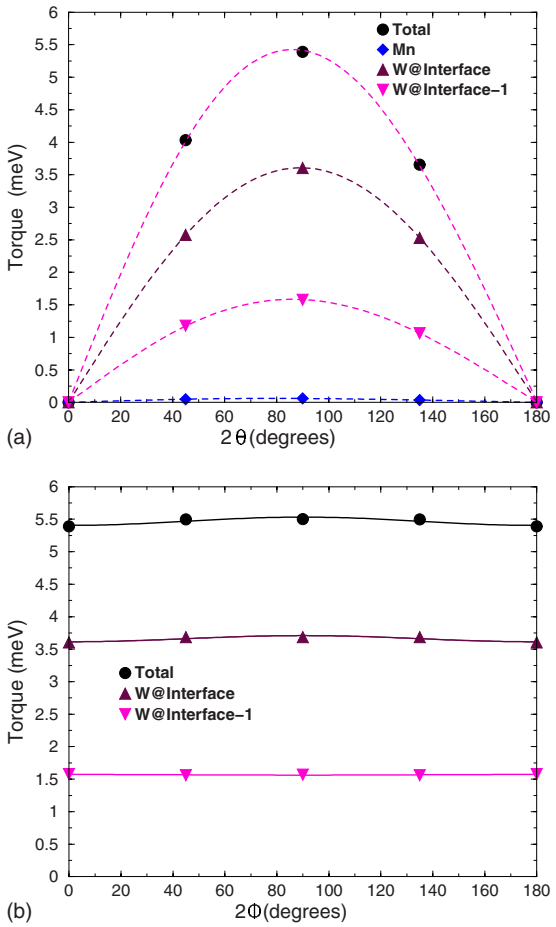

FIG. 2. (Color online) The torque $T(\theta,\phi)$ for the x-z plane ($\phi = 0$) (a) as a function of θ and as (b) a function of ϕ for $\theta = 45°$. The leading contributions from the Mn top layer, W interface layer, and W subinterface layer are shown. Equation (2) is used to fit the torque angular dependence.

$$E(\theta,\phi) = K_2 \sin^2(\theta) + K_{4\perp} \sin^4(\theta) + K_{4\parallel} \sin^4(\theta)\cos(4\phi), \tag{1}$$

where K_2 is the uniaxial MAE constant, and $K_{4\perp}$ and $K_{4\parallel}$ are the fourth-order out-of-plane and in-plane MAE constants,[22] respectively. The angular dependence of the torque is then given by

$$T(\theta,\phi) = K_2 \sin(2\theta) + 2[K_{4\perp} + K_{4\parallel} \cos(4\phi)]\sin^2(\theta)\sin(2\theta). \tag{2}$$

Microscopic values of the total and element specific anisotropy constants are shown in Table II, focusing on the main contributions coming from the Mn top layer, W interface layer, and W subinterface layer. The uniaxial constant K_2 is dominated by contributions from the W layers at the Mn/W interface and subinterface. For the out-of-plane constant $K_{4\perp}$, the role of W at the interface is almost negligible but increases for the subinterface layer. The contribution to the in-plane constant $K_{4\parallel}$ decreases when moving away from the interface. As expected for our highly anisotropic layered

TABLE II. The uniaxial K_2, and fourth-order out-of-plane and in-plane $K_{4\perp}$, $K_{4\|}$-fourth-order MAE constants (meV/Mn atom) obtained from Fig. 1 and Eq. (2) for the total MAE, and element specific contributions for the Mn top layer, W interface layer [W(I)], and W subinterface layer [W(I-1)].

	Total	Mn	W(I)	W(I-1)
K_2	5.79	0.07	3.65	1.69
$K_{4\perp}$	−0.32	0.00	0.00	−0.12
$K_{4\|\|}$	−0.06	0.00	−0.05	0.01

structure, the uniaxial MAE substantially (by a factor of 20) exceeds the fourth-order MAE terms.

The torque calculations yield the Mn-atom contribution to the uniaxial MAE of $K_2=0.07$ meV. It is by a factor of 2 smaller than the uniaxial MAE of 0.16 meV estimated from the Bruno formula,[23] $\mathrm{MAE}\approx-\xi/4(M_L^x-M_L^z)$, where we use the value of the Mn-atom SOC constant $\xi=45$ meV and the anisotropy of M_L of $-0.014\mu_B$ (see Table I). It has been shown by van der Laan[24] that the MAE expression in Ref. 23 is incomplete and neglects the spin-off-diagonal contributions to the MAE. Moreover, the Bruno formula treats the SOC perturbatively and in the case of the 3*d*-5*d* bimetallic systems with strong SOC represents very crude approximation only.

The large difference between Mn and W uniaxial MAE contributions is not surprising and the ratio $K_2(\mathrm{W})/K_2(\mathrm{Mn})=52$ at the interface directly corresponds to the ratio $(\xi_{\mathrm{W}}/\xi_{\mathrm{Mn}})^2=50$ of the W and Mn atoms SOC constants. Away from the interface, the W contribution to the uniaxial MAE decreases along with the decreasing induced moment (see Table I).

An important feature of the bimetallic Mn/W system is that itinerant 5*d*(W) magnetic moments $\mathbf{M}^{5d}$ are induced by the exchange field due to strongly localized 3*d*(Mn) moments $\mathbf{M}^{3d}$ so that we can write[25]

$$\mathbf{M}^{5d}=\chi\sum_i J^i_{3d\text{-}5d}\mathbf{M}^{3d}_i, \tag{3}$$

where the sum runs over 3*d* atoms, $J^i_{3d\text{-}5d}$ is the exchange between the *i*th 3*d*(Mn) atom and the 5*d*(W) atom, and χ is the 5*d*-atom local-spin susceptibility. The uniaxial MAE [see Eq. (1)] contribution from the 5*d*(W) atom, $E_A^{5d}=-k_2^{5d}(M^{5d,z})^2$, can be then written using Eq. (3) as

$$E_A^{5d}=-k_2^{5d}\chi^2\sum_{ij}J^i_{3d\text{-}5d}J^j_{3d\text{-}5d}M_i^{3d,z}M_j^{3d,z}, \tag{4}$$

where the renormalized anisotropy constant k_2^{5d} is proportional to ξ_{5d}^2.

Equation (4) shows, that the large uniaxial anisotropy in various 3*d*-5*d* bimetallic systems, including the technologically important CoPt and FePt, originates from a combination of strong 5*d* SOC (k_2^{5d}), strong exchange splitting induced by the 3*d* magnetic element ($J_{3d\text{-}5d}\mathbf{M}^{3d}$), and the enhancement of the local-spin susceptibility χ. All these criteria are important in the quest for new highly anisotropic bimetallic alloys and nanostructures.

D. Density of states anisotropy

Our theoretical discussion of the ferromagnetic Mn/W(001) model system from the perspective of the differential TAMR effect follows the approach applied previously to Co/Pt TAMR devices.[7,10] The analysis is based on calculating DOS anisotropies in the ferromagnetic electrode with respect to the orientation of the magnetic moment and assumes proportionality between the DOS and the differential tunneling conductance anisotropies. It is to mention that the use of the DOS anisotropy in evaluating the differential TAMR can serve only as a very crude approximation which assumes that the product of tunneling matrix elements to the DOS of nonmagnetic electrode stays constant.[26]

The band structures are obtained, as in the MAE calculations, within the local–spin-density approximation using the relativistic version of the FP-LAPW method in which SOC is included in a self-consistent second-variational procedure. The magnetic force theorem is used to evaluate the DOS anisotropies which result from SOC induced changes in the band eigenvalues. In order to increase the accuracy in DOS evaluation, the smooth Fourier interpolation scheme is used together with the linear tetrahedron method.[27]

The calculated DOS of the Mn/W(001) structure as a function of energy measured from the Fermi level are shown in Fig. 3(a) for the in-plane (x) and out-of-plane (z) magnetization orientations. We find a complex structure of the DOS near the Fermi energy with the main features shifted by ~0.1 eV for two different magnetization directions. The corresponding DOS anisotropy $[\mathrm{DOS}(M\|z)\text{-}\mathrm{DOS}(M\|x)/\mathrm{DOS}(M\|x)]$ is shown in Fig. 3(b). This DOS anisotropy, related to the differential conductance anisotropy of a TAMR device, shows an oscillatory behavior as a function of energy. The magnitude reaches ~100% which is nearly an order of magnitude larger than in the previously theoretically and experimentally studied TAMR devices with the Co/Pt magnetic electrode.

E. Curie temperature and recording density

We conclude our theoretical discussion of the ferromagnetic Mn/W(001) system with the strong uniaxial anisotropy by estimating semiquantitatively the Curie temperature T_c and the magnetic recording density that can be achieved in this model structure. Using the random-phase approximation (RPA),[28] the spin-wave energy and T_c are given by[29]

$$E(\mathbf{q})=\frac{4}{M}\sum_{j\neq0}J_{0j}[1-\exp(i\mathbf{q}\mathbf{R}_{0j})]+\Delta,$$

$$\frac{1}{k_BT_c}=\frac{6}{M}\frac{1}{N}\sum_{\mathbf{q}}^{\mathrm{BZ}}\frac{1}{E(\mathbf{q})}. \tag{5}$$

Here, the $\mathbf{q}$ sum extends over the 2D-BZ, R_{0j} is the interatomic distance, M is the magnetic moment per atom (in μ_B), and Δ is the total uniaxial MAE per atom (with the shape anisotropy included).

The exchange interactions in Eq. (5) are evaluated using the approach of Ref. 25. The Mn-Mn exchange interactions

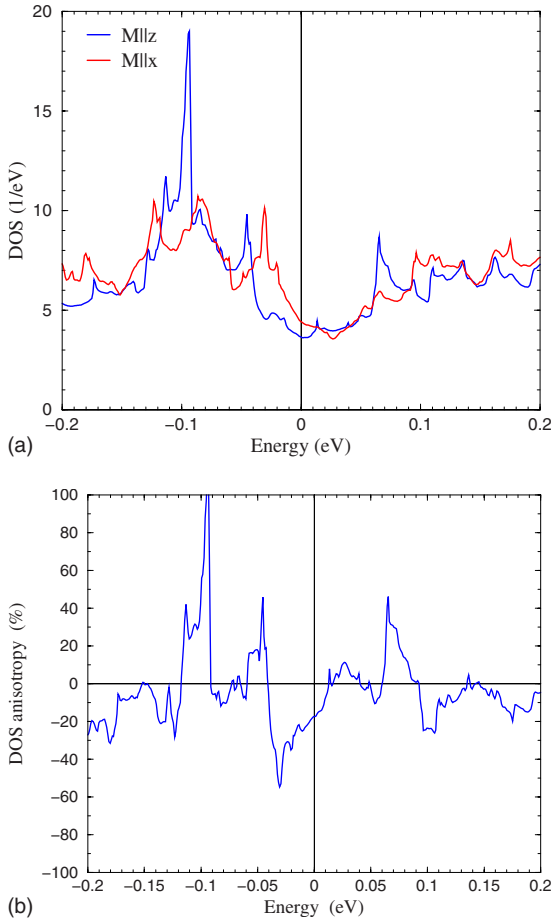

FIG. 3. (Color online) (a) Total DOS for $M\|z$-axis and $M\|x$ axis. (b) The DOS anisotropy $[\mathrm{DOS}(M\|z)\text{-}\mathrm{DOS}(M\|x)/\mathrm{DOS}(M\|x)]$ as a function of energy measured form the Fermi level.

rapidly decay with increasing interatomic distance. Keeping only the leading first-nearest-neighbor $J_{01}=22.78$ meV and second-nearest-neighbor $J_{02}=-7.11$ meV Mn-Mn exchange interactions, expanding the exponents in Eq. (5) up to the q^2 terms and taking into account uniaxial anisotropy constant $K_2=5.79$ meV/Mn atom (see Table II) plus the shape anisotropy $E_{\mathrm{dd}}=-0.12$ meV/Mn atom, we obtain the Curie temperature $T_c\approx 655$ K. The large uniaxial MAE contributes significantly to this relatively high value of T_c.

Finally, we estimate the magnetic recording density limit which would correspond to the MAE of the considered Mn/W(001) system. We use the standard criterion $\Delta N/k_BT(\mathrm{room})=60$ (Ref. 30) needed to ensure the thermal stability of the information bit for 10 years. It yields $N\sim 275$ Mn atoms in the information bit with corresponding areal density of $\sim 22\times 10^{12}$ bit/in.^{2}.

III. CONCLUSIONS

In this paper we have considered only the collinear magnetic structure of Mn/W(001). It is now established[31] that due to the broken inversion symmetry at the surface, the anisotropic Dzialoshinskii-Moria (DM) exchange interaction can induce a noncollinear chiral magnetic ordering. The experimental evidence of these long-period chiral magnetic structures with the period of ~40 interatomic distances has recently been reported for the anti-FM Mn overlayer on the W(110) surface.[32] The DM-induced chiral structures can also form at FM-ordered surfaces with the uniaxial MAE.[33] We have omitted these effects in our model calculations. We emphasize that similarly strong anisotropy effects are expected when considering Mn/W multilayers, instead of a single Mn overlayer, which restore the inversion symmetry and therefore make the DM interaction ineffective.

To conclude, our first-principles calculations revealed unusually large uniaxial MAE and DOS anisotropies in the ferromagnetic Mn overlayer on W(001). This makes structures based on Mn/W(001), as well as other bimetallic systems with optimally balanced conditions to maximize moment on the magnetic $3d$ atom, exchange coupling between the $3d$ and $4(5)d$ elements, and magnetic susceptibility and spin-orbit coupling of the $4(5)d$ metal, promising candidates for both high-density magnetic recording and TAMR applications.

ACKNOWLEDGMENTS

We acknowledge support from the Academy of Sciences of the Czech Republic under Grants No. AV0Z10100520 and No. AV0Z10100521, from the Grant Agency of the Czech Republic under Grants No. FON/06/E002, No. 202/07/0456, and No. 202/07/0644, from the Czech Ministry of Education under Grant No. LC510, from the EU Grant No. IST-015728, and from the U.S. Grant SWAN-NRI. O.N.M. acknowledges the SFI C. T. Walton Foundation support during his stay at Trinity College, Dublin.

[1] T. Burkert, L. Nordstrom, O. Eriksson, and O. Heinonen, Phys. Rev. Lett. **93**, 027203 (2004).
[2] G. Andersson, T. Burkert, P. Warnicke, M. Bjorck, B. Sanyal, C. Chacon, C. Zlotea, L. Nordstrom, P. Nordblad, and O. Eriksson, Phys. Rev. Lett. **96**, 037205 (2006).
[3] P. Gambardella, A. Dallmeyer, K. Maiti, M. Malagoli, W. Eberhardt, K. Kern, and C. Carbone, Nature (London) **416**, 301 (2002); P. Gambardella *et al.*, Science **300**, 1130 (2003).
[4] C. Gould, C. Ruster, T. Jungwirth, E. Girgis, G. M. Schott, R. Giraud, K. Brunner, G. Schmidt, and L. W. Molenkamp, Phys. Rev. Lett. **93**, 117203 (2004).
[5] L. Brey, C. Tejedor, and J. Fernandez-Rossier, Appl. Phys. Lett. **85**, 1996 (2004).
[6] M. Ciorga, M. Schlapps, A. Einwanger, S. Geissler, J. Sadowski, W. Wegscheider, and D. Weiss, New J. Phys. **9**, 351 (2007).
[7] A. B. Shick, F. Máca, J. Mašek, and T. Jungwirth, Phys. Rev. B **73**, 024418 (2006).
[8] J. Moser, A. Matos-Abiague, D. Schuh, W. Wegscheider, J. Fa-

bian, and D. Weiss, Phys. Rev. Lett. **99**, 056601 (2007).
[9] L. Gao, X. Jiang, S.-H. Yang, J. D. Burton, E. Y. Tsymbal, and S. S. P. Parkin, Phys. Rev. Lett. **99**, 226602 (2007).
[10] B. G. Park, J. Wunderlich, D. A. Williams, S. J. Joo, K. Y. Jung, K. H. Shin, K. Olejnik, A. B. Shick, and T. Jungwirth, Phys. Rev. Lett. **100**, 087204 (2008).
[11] P. Ferriani, S. Heinze, G. Bihlmayer, and S. Blugel, Phys. Rev. B **72**, 024452 (2005).
[12] G. Kresse and J. Hafner, Phys. Rev. B **47**, 558 (1993); G. Kresse and J. Furthmüller, Comput. Mater. Sci. **6**, 15 (1996); G. Kresse and D. Joubert, Phys. Rev. B **59**, 1758 (1999).
[13] S. Dennler and J. Hafner, Phys. Rev. B **72**, 214413 (2005).
[14] D. J. Singh, *Planewaves, Pseudopotentials and the LAPW Method* (Kluwer, Boston, 1994), p. 115.
[15] P. Blaha, K. Schwarz, G. K. H. Madsen, D. Kvasnicka, and J. Luitz, *WIEN2k, An Augmented Plane Wave Plus Local Orbitals Program for Calculating Crystal Properties* (Karlheinz Schwarz, Technische Universitat Wien, Austria, 2001).
[16] A. B. Shick, D. L. Novikov, and A. J. Freeman, Phys. Rev. B **56**, R14259 (1997).
[17] M. Methfessel, and J. Kubler, J. Phys. F: Met. Phys. **12**, 141 (1982); A. I. Liechtenstein, M. I. Katsnelson, V. P. Antropov, and V. A. Gubanov, J. Magn. Magn. Mater. **67**, 65 (1987).
[18] F. Wilhelm, P. Poulopoulos, H. Wende, A. Scherz, K. Baberschke, M. Angelakeris, N. K. Flevaris, and A. Rogalev, Phys. Rev. Lett. **87**, 207202 (2001).
[19] L. Szunyogh, B. Ujfalussy, and P. Weinberger, Phys. Rev. B **51**, 9552 (1995).
[20] See, for review, J. Staunton, Ψ_k—network highlight, 2007.
[21] X. Wang, R. Wu, D.-S. Wang, and A. J. Freeman, Phys. Rev. B **54**, 61 (1996).
[22] S. Chikazumi, *Physics of Ferromagnetism* (Clarendon, Oxford/Oxford University Press, New York, 1997), p. 655.
[23] P. Bruno, Phys. Rev. B **39**, 865 (1989).
[24] G. van der Laan, J. Phys.: Condens. Matter **10**, 3239 (1998).
[25] O. N. Mryasov, U. Nowak, K. Y. Guslienko, and R. W. Chantrell, Europhys. Lett. **69**, 805 (2005).
[26] H. Bruus and K. Flensberg, *Many-Body Quantum Theory in Condensed Matter Physics* (Oxford University Press, New York, 2004), p. 466.
[27] W. E. Pickett, H. Krakauer, and P. B. Allen, Phys. Rev. B **38**, 2721 (1988).
[28] J. Kudrnovský, V. Drchal, I. Turek, M. Pajda, and P. Bruno, Czech. J. Phys. **52**, 215 (2002); M. Pajda, J. Kudrnovský, I. Turek, V. Drchal, and P. Bruno, Phys. Rev. Lett. **85**, 5424 (2000).
[29] A. B. Shick, F. Máca, J. Mašek, and T. Jungwirth, Phys. Rev. B **73**, 024418 (2006).
[30] D. Weller, A. Moser, L. Folks, M. E. Best, M. F. Wen Lee Toney, M. Schwickert, J.-U. Thiele, and M. F. Doerner, IEEE Trans. Magn. **36**, 10 (2000).
[31] E. Y. Vedmedenko, L. Udvardi, P. Weinberger, and R. Wiesendanger, Phys. Rev. B **75**, 104431 (2007), and references therein.
[32] M. Bode, M. Heide, K. von Bergmann, P. Ferriani, S. Heinze, G. Bihlmayer, A. Kubetzka, O. Pietzsch, S. Blügel, and R. Wiesendanger, Nature (London) **447**, 190 (2007).
[33] P. Ferriani, K. von Bergmann, E. Y. Vedmedenko, S. Heinze, M. Bode, M. Heide, G. Bihlmayer, A. Kubetzka, S. Blügel, and R. Wiesendanger, Phys. Rev. Lett. **101**, 027201 (2008).